Mechanisms of geometrical seismic attenuation

Igor B. Morozov

Department of Geological Sciences, University of Saskatchewan, Saskatoon, SK S7N 5E2 Canada

Abstract

In several recent papers, we explained the frequency dependence of the apparent seismic quality-factor (Q) observed in many studies by the effects of geometrical attenuation (GA), which was defined as the zero-frequency limit of the temporal attenuation coefficient. In particular, GA was found to be positive for most waves traveling within the lithosphere. Here, we present three theoretical models illustrating the origin of such GA, and investigate the causes of its preferential positive values. In addition, we discuss the physical basis and limitations of both the conventional and new attenuation models.

For waves in media with slowly varying properties, GA is caused by variations of wavefront curvatures, which can be both positive (for defocusing) and negative (for focusing). In media with velocity/density contrasts, incoherent reflectivity leads to GA coefficients which are proportional to the mean squared reflectivity and always positive. For "coherent" reflectivity, the GA is approximately zero, and the attenuation process can be described by the concept of "scattering Q." However, the true meaning of this parameter is in describing the mean reflectivity within the medium and not that of the traditional resonator quality factor known in mechanics.

The general conclusion from these models is that non-zero and often positive levels of GA are common in realistic, heterogeneous media both observationally and theoretically. When transformed into the conventional Q-factor form, such positive GA leads to Q values quickly increasing with frequency. These predictions show that the positive frequency dependent Q observed in many datasets may represent artifacts of the transformations of the attenuation coefficients into Q.

1. Introduction

In several recent papers [Morozov, 2008, 2009a, b, 2010a–d; hereafter referred to as M08, M09a, b, and M10a–d, respectively], we argued that the conventional description of seismic attenuation using the quality factor of the medium (denoted Q) relies on theoretical conjectures, analogies, and assumptions which are insufficiently based on the fundamental principles of mechanics. In consequence, the resulting Q models may be prone to spurious frequency dependences and lead to overly complex and ambiguous interpretations. One general manifestation of such excessive complexity may be in Q values quickly increasing with frequency, which is commonly reported, particularly in coda and total-energy studies (*e.g.*, Aki, 1980). As suggested in M09b, such increases may often be dictated by the very definition of Q used in seismology, and not related to any rheological or scattering properties of the medium. Instead of using the Q paradigm, we suggested returning to another well-known description, which is the attenuation coefficient in either its spatial (α) or temporal (χ) forms. While removing the assumptions and uncertainties involved in the definition of Q, this description provides a simple and reliable basis for data analysis [M08, M10a] and offers several far-reaching empirical generalizations [M10b].

The key message of the aforementioned papers was that for many wave types (short-and long-period surface and body waves, coda, *Pn*, *Lg*, and even the whole-Earth free oscillations), the observed variations of Q with frequency typically correspond to piecewise-linear dependences of the attenuation-coefficient, $\chi(f)$ (Figure 1). The intercept values of these dependences, denoted $\gamma \equiv \chi|_{f\to 0}$, are often positive in lithospheric measurements and correlate with tectonic types and ages of the crust [Figure 1; M08]. Slopes of these linear $\chi(f)$ segments lead to a new, "effective" quality-factor type measure, $Q_e = [(d\chi/df)/\pi]^{-1}$, which is usually frequency-independent and significantly higher than the conventional $Q_0 = Q(1\text{ Hz})$ (Figure 1). Thus, instead of the conventional pair of parameters Q_0 and η in the power law $Q(f) = Q_0 f^{\eta}$, the new description uses parameters γ and Q_e in the linear dependence:

$$\chi(f) = \gamma + \frac{\pi}{Q_e} f \ . \tag{1}$$

Although also subject to some subtleties [M10a], the basic interpretation of parameters γ and Q_e is nevertheless much more straightforward than that of Q_0 and η. This interpretation can be summarized as follows:

1) The zero-frequency limit, γ, is principally responsible for the effects of the "structure," i.e., for ray bending, lithospheric reflections and conversions, multi-pathing, and scattering not accounted for by the background model, which is used for geometrical or other types of corrections performed prior to the attenuation measurements. Because of this meaning, we often refer to parameter γ as "geometrical" [M08, M09a], although in certain cases, frequency-dependent geometrical spreading may cause complications to this terminology [M10a].

2) Parameters κ or Q_e describe the effects of anelastic attenuation and small-scale,

random scattering. In relation to γ above, we call these attenuation parameters "non-geometrical."

Notably, for at least short-period coda waves, γ can be modeled from totally independent, structural information by using numerical waveform modeling [Morozov *et al*., 2008]. By contrast, the non-geometrical parameters are unrelated to the structure, but they can be recognized by the characteristic increase of the attenuation coefficient with frequency.

In many datasets, the observed frequency-dependent values of $Q \sim f^{\eta}$, with η approaching and sometimes exceeding 1, can be explained by the presence of a significant positive "geometrical attenuation," $\gamma > 0$ (Figure 1) [M08, M10a,b]. Therefore, it appears that $\gamma > 0$ could be due to some common physical properties of the lithosphere. In the present paper, we offer some theoretical evidence for the potential causes of such values of γ. We show that positive geometrical attenuation can be caused by: 1) variations of wavefront curvatures during refraction in smoothly-varying media, and 2) by incoherent reflectivity along the wave-propagation paths. In the conventional, Q-based paradigm, such γ values could also be attributed to a strongly frequency-dependent "scattering Q," although such terminology could be misleading because of its attributing the deterministic effects of the structure to a Q [M09a, M10a]. However, in the third example below, we also consider a case of short-scale, "coherent" reflectivity, for which a kind of "scattering Q" becomes meaningful and frequency-independent.

Despite its simplicity and productive use, model (1) recently met with significant criticism [Xie and Fehler, 2009; Xie, 2010], which even led to a special forum in *Pure and Applied Geophysics* [Mitchell, 2010]. The critique touched upon a broad range of subjects but focused primarily on the perceived lack of a physical meaning of expression (1), and particularly of its geometrical part, γ. The theoretical examples developed in Section 3 answer these questions by explaining the physical rationale of the functional form (1) and illustrating the physical mechanisms and approximations involved in the concepts of χ and γ. These examples also show the practical uses and limitations of approximation (1). For readers interested in the fundamentals of the concept of Q and in further detail of this extensive debate, additional comments are given in Appendix A. Although not critical for the present article, this discussion helps in understanding the physics of the attenuation coefficient and its relation to the conventional seismic attenuation model and viscoelasticity.

2. Apparent and intrinsic attenuation coefficients

The observed (apparent) temporal attenuation coefficient, denoted χ here, was heuristically inferred in M08 and M10a,b by analyzing the seismic path factor within several frequency bands:

$$P = G_0 \delta P \text{ , where } \delta P = e^{-\chi t} . \qquad (2)$$

In these expressions, P denotes the seismic amplitude corrected for the source and receiver effects, and G_0 is the reference geometrical spreading, such as $G_0(t) = t^{-1}$ used in many local-coda studies. Factor δP is the residual of P remaining after the geometrical correction, and $e^{-\chi t}$ represents the perturbation-theory approximation for this δP. This

approximation means that G_0 is normalized so that at $t = 0$, $P = G_0$, and for $t > 0$, δP is predicted by the scattering theory [M10a]. Expression (2) represents the starting point of most attenuation measurements, in which χ is directly measured from either the time-domain logarithmic decrements of the amplitudes, or from the widths of the spectral peaks near resonances (Figure 2).

Unfortunately, χ is rarely studied by itself but usually converted into the "apparent Q" by assuming a specific form for its frequency-dependence [*e.g.*, Aki, 1980]:

$$\chi(f) = \frac{\pi f}{Q(f)}, \text{ and accordingly, } Q(f) = \frac{\pi f}{\chi(f)}. \tag{3}$$

Note that Q is never measured directly but is only derived from χ by using the second expression (3). Although appearing only as a simple scaling, the above transformation has a deep implication: it assumes that $\chi \to 0$ when $f \to 0$. However, this assumption is too restrictive and inaccurate in most practical cases. Transformation (3) assumes that attenuation occurs proportionally to the number of oscillation cycles and is meaningful only for purely oscillatory processes, such as shown in Figure 2. Nevertheless, in reality, χ often includes contributions from ray bending, reflectivity, multi-pathing, scattering, and other effects of the structure, for which $\chi|_{f\to 0} \neq 0$. In such cases, transformation (3) results in $Q(f)$ values that are nearly proportional to f, which is often observed.

To avoid the tendency of Q to spuriously increase with frequency, we do not use the restrictive model for $Q(f)$ in Equation (3) and view $\chi(f)$ as an arbitrary function. In empirical data analysis, it is useful to start by isolating its zero-frequency limit γ in $\chi(f)$ [M08]:

$$\chi(f) = \gamma + f\kappa(f). \tag{4}$$

Compared to Equation (3), the only difference of this form is in allowing γ to be non-zero. For $\gamma = 0$, Equations (3) and (4) are equivalent, which once again emphasizes the character of the assumption on which approximation (3) is based.

The dimensionless parameter κ in Equation (3) can generally be frequency-dependent; however, from several data examples [M08, M09a, M10a,b] and numerical modeling of the seismic coda [Morozov *et al*., 2008] and mantle Love waves, it turns out to be frequency-independent for many wave types and frequency bands. The only waves for which the measured κ is clearly frequency-dependent are the free oscillations of the Earth, and even for them, $\kappa(f)$ appears to break into only two linear branches of the form (3) [Figure 1; M10a]. For comparisons to the conventional terminology, κ can be transformed into an "effective" quality factor $Q_e = \pi/\kappa$ used in expression (1) [M08].

Note that the apparent χ is also closely related to parameter t^* often used in body-wave attenuation studies [*e.g.*, Der and Lees, 1985] as $\chi = \pi f t^*/t$. This parameter is usually interpreted as Q^{-1} accumulated along the ray path:

$$t^* = \int_{path} Q^{-1} dt, \tag{5}$$

where t is the propagation time. Because of its affinity to Q^{-1}, t^* also exhibits the same instability with respect to the background geometrical-spreading correction and a similar variation with frequency. For example, the values of t^* for body *P*-waves decrease from ~1 s for long-period waves to ~0.2 s at short periods [Der and Lees, 1985], which may also be a spurious (apparent) effect related to the use of the *Q*-type model of attenuation. In more detail, we discuss this point elsewhere. However, because the frequency-dependent Q^{-1} in seismology is essentially used as a proxy for χ (Equation 3), χ can also be represented by a path average of the corresponding "intrinsic attenuation coefficient," χ_i [M10b]:

$$\chi = \frac{1}{t}\int_{path} \chi_i d\tau \,. \tag{6}$$

This new quantity combines local variations of geometrical spreading, scattering, and anelastic attenuation within the medium. Of these three factors, the anelastic attenuation is the one that definitely requires a frequency-dependent χ_i (compare to Equation 3). As argued in detail in M10a, the other two factors can only be separated by making additional simplifications, such as assuming a frequency-independent residual geometrical spreading. The difficulty of their separation is related to the fundamental ambiguity in the definitions of the geometrical spreading and scattering. However, in many practical cases including the present paper, separation of these quantities is not required, and χ_i can be treated as a single medium property.

The most important observation from Equations (2) and (6) is that for traveling waves, δP represents a path integral, which can be rendered in either the temporal or spatial forms:

$$\delta P = \exp\left(-\int_{path} \chi_i dt\right) = \exp\left(-\int_{path} \alpha_i ds\right), \tag{7}$$

where s is the ray path length, and α_i and χ_i are is the corresponding spatial and temporal intrinsic attenuation coefficients. This shows that the variations of geometrical spreading, scattering, and attenuation have similar characters and are accumulated over the wave propagation paths. The exponential form possesses important general properties and similarities to ray-, wave-, and quantum-field mechanics.

3. Models for geometrical attenuation

In this section, we consider three theoretical examples illustrating the path-integral forms (7) for χ and showing what mechanisms could create the linear frequency dependences of χ (Equation 3). As we will see, the residual geometrical spreading γ_i and the corresponding frequency-independent κ_i occur in several end-member cases:

1) Refraction in a medium with smoothly varying velocities. This example shows that γ_i is also related to the variations of wavefront curvature (*i.e.*, to perturbations of the traditional geometrical spreading).

2) Incoherent normal-incidence reflectivity, corresponding to large numbers of sparse reflections occurring during long propagation paths. In this case, χ_i is proportional to the gradient of the acoustic impedance.

3) Short-scale reflectivity, with random but "coordinated" (alternating) reflectivity at scale-lengths much shorter than the length of the incident wave. In this case, the reflectivity becomes "coherent" at $f \to 0$, and consequently $\gamma_i = 0$. This example is studied numerically, as in Richards and Menke [1983].

All these cases relate to the elastic processes of refraction or reflectivity, which fall under the category of "scattering," or more generally, "geometrical" attenuation processes discussed in M08 and M10a. Our specific goal here is to illustrate the origins of the geometrical parameter γ_i in theoretically-tractable cases. The physics of anelastic attenuation is not discussed in these examples, and its effects are simply incorporated by the additional factor $\exp(-\kappa_i f t)$.

3.1 Variations of wavefront curvature

The dynamic ray theory [Červený, 2001] illustrates the origins of the exponential form (7) for the attenuation coefficient. In this theory, the wave-amplitude variation is described by the ray propagator Π, which in logarithmic form is [Equation 4.4.86 in Červený, 2001]:

$$\ln \Pi\left(R,S\right) = \ln \Pi\left(R,\tilde{Q}_N\right) + \sum_{i=1}^{N} \Upsilon\left(\tilde{Q}_i,\tilde{Q}_{i-1}\right). \tag{8}$$

Here, S is the source, R is the receiver, and Q_i and $\tilde{Q}_i$ are the incidence and emergence points at the i-th interface, respectively (Figure 3), and

$$\Upsilon\left(\tilde{Q}_i,\tilde{Q}_{i-1}\right) = \ln\left[\Pi\left(\tilde{Q}_i,Q_i\right)\Pi\left(Q_i,\tilde{Q}_{i-1}\right)\right]. \tag{9}$$

In our notation (Equation 7), δP corresponds to $\Pi(R,S)$, and $\Upsilon\left(\tilde{Q}_i,\tilde{Q}_{i-1}\right)$ equal to $\int \chi_i d\tau$, where χ_i is the intrinsic attenuation coefficient, and the integral is taken from point Q_{i-1} to Q_i along the ray.

In the absence of interfaces and caustics, the geometrical spreading is caused by the variations in the waveform curvature (Figure 3). In the dynamic ray theory, this curvature is denoted H and measured by the trace of the wavefront curvature matrix, $\mathbf{K}$: $H = \frac{1}{2}$ tr $\mathbf{K}$. Matrix $\mathbf{K}$ consists of second derivatives of the travel-time field T with respect to the wavefront-orthonormal coordinates y_k [Equation 4.6.15 in Červený, 2001]:

$$K_{ij} = V \frac{\partial^2 T}{\partial y_i \partial y_j}, \tag{10}$$

where V is the wave velocity. Wavefront curvature H is related to the ray-theoretical geometrical spreading, $G_0 \propto L^{-1}$, by the following differential equation [Equations 4.10.28–29 in Červený, 2001]:

$$H = L^{-1}\frac{dL}{ds}, \tag{11}$$

where L is the geometrical-spreading denominator, and s is the ray arc length. The solution to this equation relating $L(R)$ at the receiver to $L(S)$ at the source is

$$L(R) = L(S)\exp\left(\int_S^R H ds\right), \tag{12}$$

which has the expected exponential path-integral form of Equation (7). Ratio $G = L(S)/L(R)$ represents the geometrical spreading factor, which equals $G_0\delta P = \exp(-\alpha_i s)$. In the presence of anelastic attenuation given by parameter κ_i, the full path factor becomes:

$$\delta P = \frac{1}{G_0}\frac{L(S)}{L(R)}\exp\left(-f\int_S^R \frac{\kappa_i ds}{V}\right), \tag{13}$$

and by writing this expression in terms of the intrinsic spatial attenuation coefficient, α_i,

$$\delta P = \exp\left(-\int_S^R \alpha_i ds\right), \tag{14}$$

we see that α_i equals in this case:

$$\alpha_i = H - \ln G_0 + \frac{\kappa_i}{V_i} f\ , \tag{15}$$

with the corresponding relation for $\chi_i = \alpha_i V$. These expressions show that for smoothly-refracting waves, α_i contains a frequency-independent "geometrical" part (H-lnG_0), which equals the difference of the actual wavefront curvature from the one predicted by the geometrical-spreading law selected as the background reference.

3.2 Incoherent reflectivity

To understand the relation of the in-situ attenuation coefficient to the properties of the medium, it is instructive to analyze its properties in a simple 1-D medium. For plane-wave propagation, the theoretical geometrical-spreading factor G_0 equals one; however, reflections within a heterogeneous medium cause deviations from this level. Because the transmission coefficients are completely described by the reflection-coefficient series, the geometrical part of the attenuation coefficient should also be related to reflectivity. In fact, as shown below, the geometrical attenuation coefficient equals half of the average

squared reflection coefficient.

To begin, consider a boundary between two layers of acoustic impedances Z_{j-1} and Z_j (Figure 4). The specific expression for impedance depends on the local properties of the medium, wave type, and the angle of its incidence on the boundary. From [M10c], in the presence of attenuation, the complex-valued acoustic impedance for a *P*- or *S* wave at normal incidence is

$$Z = \rho V\left(1+\frac{i}{2Q_i}\right), \tag{16}$$

where ρ, V, and Q_i^{-1} are the mass density, wave velocity, and parameter of anelastic attenuation, respectively. Note that although we generally argue that Q cannot be considered as a medium property, this parameter is retained here for convenience of comparison to the current terminology. Such use of anelastic Q is possible because we are considering an otherwise uniform background, in which the geometrical spreading is accurately known, a single wave type is used, and therefore Q appears in its specific, phenomenological sense of a plane-wave amplitude decay parameter [M09b].

Considering for simplicity the normal-incidence case and denoting the displacement in the incident wave by u, the displacements in the reflected and transmitted waves become $(-R_i u)$ and $T_i u$, respectively (Figure 4), where, R_i is the reflection coefficient,

$$R_j = \frac{Z_j - Z_{j-1}}{Z_j + Z_{j-1}}, \tag{17}$$

and $T_j = 1 - R_j$ is the transmission coefficient,

$$T_j = \frac{2Z_{j-1}}{Z_j + Z_{j-1}}. \tag{18}$$

The corresponding transmission coefficient for energy is

$$T_{E,j} = \frac{Z_j}{Z_{j-1}}T_j^2 = \frac{4Z_{j-1}Z_j}{\left(Z_j + Z_{j-1}\right)^2}, \tag{19}$$

and the energy reflection coefficient equals $R_{E,j} = 1 - T_{E,j}$.

For small impedance contrasts, the above coefficients are:

$$R_j = \frac{1}{2}\delta_j\left(\ln Z\right), \tag{20}$$

$$T_j = 1 - \frac{1}{2}\delta_j\left(\ln Z\right), \tag{21}$$

$$T_{E,j} = 1 - \frac{1}{4}\left|\delta_j\left(\ln Z\right)\right|^2 = 1 - \left|R_j\right|^2, \tag{22}$$

where $\delta_j(X)$ denotes the contrast in quantity X across the j-th boundary. Switching to a continuous $Z(t)$ description, the impedance contrasts over an infinitesimal propagation time interval $[t,t+\delta t]$ can be considered small, and therefore from Equation (22),

$$\ln T_E \approx -\sum_{j=1}^{N}\left|R_j\right|^2 = -\int_t^{t+\delta t}\left|r\right|^2 d\tau\,, \tag{23}$$

where $r(t)$ is the root-mean square (RMS) density of reflectivity.

Equation (23) only gives the transmission loss caused by reflections on the boundaries passed by the wave between propagation times t and $t + \delta t$. The anelastic medium attenuation over the same time interval leads to an additional energy decay:

$$\ln T_E \approx -\int_t^{t+\delta t}\left|r\right|^2 d\tau - 2f\int_t^{t+\delta t}\kappa_i d\tau\,, \tag{24}$$

where κ_i is the non-geometrical attenuation factor.

If the transmitted waves interfere incoherently, the energy transmission coefficients combine multiplicatively over propagation time, and therefore their logarithms are additive. For a wave traversing N boundaries in a finite propagation time t, the energy density $E(t)$ is (Figure 4)

$$E_N = E_0\prod_{j=1}^{N}T_{E,j} = E_0\exp\left[\sum_{j=1}^{N}\ln T_{E,j}\right], \tag{25}$$

or in terms of the continuous reflectivity function, $r(t)$,

$$E\left(t\right) = E\left(0\right)\exp\left\{-\int_{\tau=0}^{t}\left[\left|r\right|^2 + 2\kappa_i f\right]d\tau\right\} \tag{26}$$

This expression shows that the logarithm of the transmitted energy loss is given by a path integral,

$$\ln E\left(t\right) - \ln E\left(0\right) = -\int_0^t\left[\left|r\right|^2 + 2\kappa_i f\right]d\tau\,, \tag{27}$$

and consequently the temporal attenuation coefficient equals

$$\chi_i = -\frac{1}{2}\frac{d\ln E(t)}{dt} = \frac{|r|^2}{2} + \kappa_i f \ . \tag{28}$$

The corresponding spatial attenuation coefficient equals $\alpha = \chi/V$:

$$\alpha_i = \frac{|r|^2 + \kappa_i}{2V} = \frac{|r_{\text{spatial}}|^2}{2} + \frac{\kappa_i}{V} f \ . \tag{29}$$

Equations (28) and (29) also show the difference between the temporally- and spatially-averaged RMS reflectivities, which are denoted by r and r_{spatial}, respectively.

Thus, for incoherent 1-D acoustic-wave propagation, the geometrical attenuation coefficient equals half the corresponding path-averaged squared reflectivity. As path-averaged properties, α and χ can be evaluated over finite propagation-time intervals, and therefore they can also be time-dependent.

Note that when $\kappa_i = 0$, the resulting α_i or χ_i are associated with geometrical attenuation, which is the zero-frequency forward scattering in this case. In the approximation considered here (normal incidence and absence of multiple reflections), these geometrical α or χ are independent of the frequency and the incident wavelength.

If multiple reflections are present, frequency-dependent effects (tuning) should arise even in the geometrical limit. Such effects should likely have the form of resonance peaks rather than a continuous trend with frequency. Such undulations of the recorded amplitudes with frequency ("spectral scalloping") on top of the linear trend of $\chi(f)$ (Equation 4) are commonly observed, as shown in several data examples recently reviewed in [M08, M10a, b].

3.3 Coherent reflectivity

The preceding example assumed incoherent interference of scattered arrivals, which occurs at all scales, but particularly when the scatterers are large and spaced at large distances compared to the incident wavelength. In this section, we consider the opposite limit of scatterers that are small and relatively closely spaced. In this case, destructive interference of scattered waves occurs, and the attenuation coefficient exhibits strong frequency dependence. For simplicity, we again consider the 1-D case, in which scattering reduces to normal-incidence reflectivity. Originally, this example was analyzed by Richards and Menke [1983], who demonstrated the frequency-dependent effects of scattering (Figure 5) and presented them in terms of the "scattering Q". Let us briefly review this important example from a somewhat different angle, and in particular look closely at the decay of the spectral amplitudes with time.

During one-dimensional propagation, the wavefronts remain perfectly planar, and consequently the theoretical geometrical spreading equals exactly 1. Therefore, all perturbations of the wavefield are due to elastic scattering on the boundaries and

anelastic attenuation between them. In particular, scattering causes a part of the wave energy to reflect backward (which is often called "back-scattering"), and a part of it continues propagating forward while being delayed relative to the primary wave. This delayed part of the propagating wavefield is called "forward-scattered" (Figure 6). From numerical simulations and real data, the initial wave pulse and both the forward- and back-scattered waves exhibit linear spectral variations, which increase with propagation time. Note that the senses of these variations are opposite for the initial pulse and back-scattered and forward-scattered waves, whose high frequencies are progressively depleted and enhanced, respectively (Figure 5).

Conventionally [for example, Richards and Menke, 1983], the relative changes in the spectra (Figure 5) are viewed as proportional to the number of wavelengths traveled by the incident wave, as in Equation (3). The resultant spectra are fit by using approximations of the form $\exp(-\pi ft/Q_s)$, and scattering is automatically viewed as analogous to the anelastic attenuation, for which the corresponding spectral amplitude decay is $\exp(-\pi ft/Q_i)$. However, as shown below, the proportionality to the number of wavelengths is incidental and only valid for coherent superposition of scattered waves. By contrast, for incoherent scattering, the attenuation tends to be independent of the incident wavelength. We therefore take a conservative view and use the Q-type parameters only for the frequency-dependent part of the attenuation coefficient.

To derive the attenuation coefficient for the general case including both weak and strong, back- and forward scattering, note that the scattering problems for both the single- and multi-boundary cases (Figure 6) can be described equivalently by using the scattering-matrix formulation:

$$\begin{pmatrix} u_+^N \\ u_-^N \end{pmatrix} = \mathbf{T}_{N,1} \begin{pmatrix} u_+^1 \\ u_-^1 \end{pmatrix} \tag{30}$$

where $N = 2$ for the 1-boundary case, and $\mathbf{T}_{N,1}$ is the transmission matrix relating the states on the right to those on the left in Figure 6. Here, u denotes the scalar wave amplitudes, waves with subscripts '$_+$' travel to the right, and those with '$_-$' travel to the left. For a single interface, transmission matrix $\mathbf{T}_{2,1}$ combines coefficients (17) and (18) for forward- and backward wave propagation,

$$\mathbf{T}_{2,1} = \frac{1}{2Z_2} \begin{pmatrix} Z_1 + Z_2 & Z_1 - Z_2 \\ Z_1 - Z_2 & Z_1 + Z_2 \end{pmatrix} \approx \mathbf{I} - \begin{pmatrix} 0 & r_2 \\ r_2 & 0 \end{pmatrix} \approx \exp\left[-\begin{pmatrix} 0 & r_2 \\ r_2 & 0 \end{pmatrix} \right], \tag{31}$$

where the second equation corresponds to the small-reflectivity approximation, r_2 is the reflectivity at the boundary, and $\mathbf{I}$ is the identity matrix. Alternately, the amplitudes of the waves traveling away from the boundary can be related to those incident on it from both sides:

$$\begin{pmatrix} u_-^1 \\ u_+^N \end{pmatrix} = \mathbf{S}_{N,1} \begin{pmatrix} u_+^1 \\ u_-^N \end{pmatrix}. \tag{32}$$

In this expression, $\mathbf{S}_{N,1}$ is called the scattering matrix. For $N = 2$, this matrix combines the reflection and transmission coefficients in both propagation directions:

$$\mathbf{S}_{2,1} = \frac{1}{Z_1 + Z_2} \begin{pmatrix} Z_2 - Z_1 & 2Z_2 \\ 2Z_1 & Z_1 - Z_2 \end{pmatrix}. \tag{33}$$

In the absence of anelastic attenuation, the elastic energy is preserved in the outgoing states:

$$Z_1 \left[\left| u_-^1 \right|^2 + \left| u_+^N \right|^2 \right] = Z_2 \left[\left| u_+^1 \right|^2 + \left| u_-^N \right|^2 \right], \tag{34}$$

for any N, and consequently the sum of powers of back- and forward-traveling waves is constant at any frequency.

For N–1 interfaces, matrix $\mathbf{T}_{N,1}$ is a product of wave-mode transformations on all boundaries:

$$\mathbf{T}_{N,1} = \prod_{i=2}^{N} \mathbf{T}_{i,i-1} \begin{pmatrix} e^{i\Delta\varphi_i} & 0 \\ 0 & e^{-i\Delta\varphi_i} \end{pmatrix} \approx \exp\left[-\sum_{i=2}^{N} \begin{pmatrix} 0 & r_i e^{i\Delta\varphi_i} \\ r_i e^{-i\Delta\varphi_i} & 0 \end{pmatrix} \right], \tag{35}$$

where $\Delta\varphi_i$ is the phase shift of the forward-traveling wave during its propagation in layer i. Let us denote the elements of this "propagator" matrix across the stack of all N–1 boundaries (Figure 6b) by

$$\mathbf{T}_{N,1} \equiv \begin{pmatrix} G^{++} & G^{+-} \\ G^{-+} & G^{--} \end{pmatrix}. \tag{36}$$

The total reflection amplitude, u_-^1, can be found from the requirement that in the right-hand side of Figure 6b, there should be no incoming wave traveling to the left:

$$u_-^2 = G^{-+} u_+^1 + G^{--} u_-^1 = 0, \tag{37}$$

and consequently

$$u_-^1 = -\frac{G^{-+}}{G^{--}} u_+^1. \tag{38a}$$

This gives the total back-scattered amplitude. The total transmitted amplitude is therefore

$$u_+^N = G^{++}u_+^1 + G^{+-}u_-^1 = \left(G^{++} - \frac{G^{+-}G^{-+}}{G^{--}} \right) u_+^1 . \qquad (38b)$$

Equation (38) can be used numerically to model the propagation of a long seismic wave through a stack of thin random layers. We use an example similar to that by Richards and Menke [1983], with 1000 layers of uncorrelated random velocities drawn from a Gaussian distribution with a mean of 3.0 km/s and standard deviation of 0.25 km/s. The density is assumed constant. Using its scale-invariance, the impedance was normalized to a mean value of $Z = 1$, and the same value of impedance was placed at both ends of the random sequence (Figure 7). The travel-time within each layer is taken equal 1 s, which also gives the characteristic Nyquist frequency of $f_N = 0.5$ Hz, relative to which all frequencies in the propagation process can be measured.

To investigate the time "history" of scattering, the impedance time series (Figure 7) was truncated at boundaries $N = 2,3,\ldots 1000$, and the remainders of the series were closed with a layer having $Z = 1$. The resulting variations of the reflected and transmitted wave intensities showed great fluctuations for the different statistical realizations of the impedance time series (Figure 8). However, after averaging over multiple realizations, the transmitted and reflected powers exhibited clear and mutually complementary exponential decays (Figure 9). By measuring the logarithmic decrements of these decays, temporal attenuation coefficients χ were measured for selected normalized frequencies f/f_N (Figure 10).

The above procedure was performed for impedance contrasts spaced at regular time intervals $\Delta t_i = 1$ s (Figure 7) and also repeated for another set of random impedance variations in which Δt_i were randomly distributed. A log-normal distribution of Δt_i was constructed so that the average $<\Delta t_i>$ also equaled 1 s. As expected, the resulting attenuation coefficients are similar for low frequencies $f < 0.3f_N$. At $f > 0.3f_N$, the attenuation in the random-Δt_i sequence saturates at a constant level (black line in Figure 10), but the attenuation in the regularly-spaced sequence continues to increase to $f \approx 0.5f_N$, after which it decreases to near-zero at $f \approx f_N$. Such pattern resembles the well-known "frequency folding" effect, which is characteristic for aliasing. As one can see, near $f \approx f_N$, phases of all reflections superimpose equivalently to the case of $f \approx 0$, and the elastic attenuation drops to zero. Interestingly, the regularly-spaced impedance series exhibits a very narrow "notch" at $f \approx 0.5f_N$, at which the attenuation drops sharply because of tuning of the incident wave with the reflectivity sequence (Figure 10). However, neither aliasing nor tuning are present in the more realistic random-Δt_i impedance series.

In summary, the general behavior of the attenuation coefficient in 1-D random media can be described as follows:

1) At near-zero frequencies, the attenuation is low ($\chi \approx 0$) because of the destructive interference of the impedance contrasts;

2) Up to certain frequency f_0, χ increases almost linearly with f. In this range, "scattering Q_s" can be meaningfully defined as $Q_s = \pi f/\chi$. However, this Q_s is not a true "quality factor" but only a measure of the slope of the $\chi(f)$ dependence, which is proportional to the mean stochastic reflection amplitude. The value of f_0 may generally depend on the statistics of the distribution of layer thicknesses and equals ~$0.3f_N$ in our example;

3) At frequencies $f > f_0$, the process of scattering becomes incoherent, and χ becomes frequency-independent.

The value of f_0 for a particular area may not be easy to determine; nevertheless, for an average sedimentary layering of ~10-cm thickness, f_0 may be quite high (~40 kHz). Therefore, the entire seismological frequency band might lie within the "scattering Q" regime for such layering and exhibit a nearly frequency-independent Q_s. However, at significantly lower frequencies and longer scale-lengths, the 1-D approximation considered here breaks down because of the effects of the structure (*i.e.*, geometrical attenuation), the attenuation coefficient saturates (Figure 10), and an apparent frequency-dependent Q_s is observed. Thus, separation of the deterministic and stochastic wave-propagation regimes is critical when considering scattering, but it cannot be done from coda data alone.

4. Discussion and conclusions

The above analysis shows that in the absence of anelastic attenuation, the resulting cumulative attenuation coefficient χ is generally non-zero and depends on the refracting or reflecting structures within which the wave propagation takes place. For refraction, the zero-frequency (geometrical) attenuation coefficients can be positive (corresponding to defocusing) or negative (focusing). For incoherent reflectivity, the geometrical attenuation coefficients are always positive. For coherent reflections in which reflections of alternating polarities occur at scale-lengths significantly smaller than the incident wavelength, the geometrical factor is approximately zero, and reflectivity can be described by "scattering Q." However, this last case is quite abstract, because an incoherent component should also be present in any random reflection sequence even in the short-scalelength case.

Thus, the non-zero limit of $\gamma \equiv \chi|_{f\to 0}$ is common in both the data and theory. This limit is explained by inaccurate knowledge and variability of the background structure. In an empirical, ad hoc interpretation staying strictly within the paradigm of Q measurements, this limit can be attributed to a "scattering Q" increasing with frequency: $Q_s = \pi f/\gamma$. However, such Q-factor terminology would ignore most of other information known about the structure, such as the existence of velocity gradients, velocity/density contrasts, bending rays, reflections, and mode conversions. On the other hand, the concept of γ correctly captures these factors in the form of the geometrical spreading associated with the structure.

The two-parameter attenuation model (1) with constant γ and Q_e considered here represents only a first-order, perturbation-theory approximation. The theoretical

examples in Section 3 indicate several limitations of this approximation, which consist in a requirement for a relatively accurate reference model G_0, weak interactions, and finite propagation times. These examples also show how these limitations can be measured and quantified. By contrast, as shown Appendix A, the conventional Q-based paradigm presents many more problems which are difficult to assess even at the level of the basic physical theory.

For unambiguous interpretation of seismic attenuation data, it is therefore important to use the attenuation-coefficient description, in which the geometrical, scattering, and anelastic-attenuation effects are treated adequately and combined in the temporal intrinsic attenuation coefficient, χ_i. Compared to this model, the emphasis on the frequency-dependent quality-factor may lead to interpretations that are overly complex but unrelated to the available structural information.

Acknowledgments

This research was supported by NSERC Discovery Grant RGPIN261610-03. GNU Octave software (http://www.gnu.org/software/octave/) was used for numerical modeling. Comments by an Associate Editor and two anonymous reviewers have helped in improving the manuscript.

References

Aki, K. (1980). Scattering and attenuation of shear waves in the lithosphere, J. Geophys. Res., 85, 6496-6504.

Aki, K. and Richards, P.G., (2002). *Quantitative Seismology*, Second Ed., University Science Books, Sausalito, California.

Biot, M. A. (1962), *Mechanics of deformation and acoustic propagation in porous media*, J. Appl. Phys. 23, 1482–1498

Bourbié, T., Coussy, O., and Zinsiger, B. (1987), *Acoustics of porous media*, Editions TECHNIP, France, ISBN 2-7108-0516-2

Carcione, J. M. (2007), *Wave fields in real media: Wave propagation in anisotropic anelastic, porous, and electromagnetic media*. Second Edition, Elsevier

Červený, V., 2001. *Seismic ray theory*, Cambridge University Press, New York, NY.

Dahlen F. A., and Tromp, J. (1998). Theoretical global seismology. Princeton Univ. Press, Princeton, NJ

Dalton, C.A. and Ekström, G. (2006), *Global models of surface wave attenuation*, J. Geophys. Res. *111*, B05317, doi:10.1029/2005JB003997

Der, Z.A., and Lees, A.C. (1985). Methodologies for estimating $t^*(f)$ from short-period body waves and regional variations of $t^*(f)$ in the United States, Geophys. J. R. Astr. Soc., 82, 125-140.

Durek J, and Ekström, G. (1996), *A radial model of anelasticity consistent with long-period surface-wave attenuation*. Bull. Seismol. Soc. Am. *86*, 155–158

Dziewonski, A. M., and Anderson, D. L. (1981), *Preliminary Reference Earth Model (PREM),* Phys. Earth Planet. Inter. *25*, 297–356

Faul, U. H., Gerald, J. D. F., and Jackson, I. (2004), Shear wave attenuation and dispersion in melt-bearing olivine polycrystals: 2. Microstructural interpretation and seismological implications, J. Geophys. Res., 109, B06202, doi:10.1029/2003JB002407.

Kinoshita, S. (1994). Frequency-dependent attenuation of shear waves in the crust of the southern Kanto area, Japan, Bull. Seismol. Soc. Am., 84, 1387–1396.

Knopoff, L. (1964), *Q*. Rev Geophys *2*, 625–660

Liu, H. P., Anderson, D. L., and Kanamori, H. (1976). Velocity dispersion due to anelasticity: implications for seismology and mantle composition, Geophys. J. R. Astr. Soc., 47, 41–58.

Mitchell, B. (2010). Prologue and invitation to participate in a forum on the frequency dependence of seismic *Q*, Pure Appl. Geophys. 167, 1129, doi 10.1007/s00024-010-0180-3

Morozov, I. B. (2008). Geometrical attenuation, frequency dependence of *Q*, and the absorption band problem. Geophys. J. Int. 175, 239–252.

Morozov, I. B. (2009a). Thirty years of confusion around "scattering *Q*"? Seism. Res. Lett. 80, 5–7.

Morozov, I. B. (2009b). On the use of quality factor in seismology. AGU Fall Meeting, San Francisco, CA, Dec 14–18, 2009, S44A-02.

Morozov, I. B. (2009c) Reply to "Comment on 'Thirty years of confusion around 'scattering *Q*'?" by J. Xie and M. Fehler, Seism, Res, Lett, 80, 648–649.

Morozov, I. B. (2010a). On the causes of frequency-dependent apparent seismological *Q*.

Pure Appl. Geophys., 167, 1131–1146, doi 10.1007/s00024-010-0100-6.
Morozov, I. B. (2010b) Attenuation coefficients of Rayleigh and *Lg* waves, J. Seismol., doi 10.1007/s10950-010-9196-5.
Morozov, I. B. (2010c) Anelastic acoustic impedance and the correspondence principle. Geophys. Prosp., doi 10.1111/j.1365-2478.2010.00890.x.
Morozov, I. B., Zhang, C., Duenow, J. N., Morozova, E.A., and Smithson, S. (2008). Frequency dependence of regional coda *Q*: Part I. Numerical modeling and an example from Peaceful Nuclear Explosions, Bull. Seism. Soc. Am., 98, 2615–2628, doi: 10.1785/0120080037
Richards, P. G., and Menke, W. (1983). The apparent attenuation of a scattering medium, Bull. Seism. Soc. Am., 75, 1005–1021.
Widmer, R., Masters, G., and Gilbert, F. (1991). Spherically-symmetric attenuation within the Earth from normal mode data, Geophys. J. Int. 104, 541–553.
Xie, J. and Fehler, M. (2009). Comment on "Thirty years of confusion around scattering *Q*" by Igor. B. Morozov, Seism. Res. Lett., 80, 646–647.
Xie, J. (2010), Can we improve estimates of seismological *Q* using a new ''geometrical spreading'' model? Pure Appl. Geophys., 167, 1147–1162, doi: 10.1007/s00024-010-0188-8.

Figure captions

Figure 1. Summary of observed $\chi(f)$ dependences for Rayleigh waves and short-period body, *Lg*, *Pn*, and coda waves. "Reduced" values of ($\chi - \pi f/1000$) are shown, so that the linear dependences corresponding to $Q_e = 1000$ appear horizontal. Typical ranges of Q_e, and γ levels discriminating between the stable and active tectonic regimes are indicated by lines and gray boxes, respectively. Modified from M10b, with permission from Springer.

Figure 2. Definition of the attenuation coefficient, χ, and quality factor, Q, for an oscillatory process in: (a) frequency-domain, (b) time-domain. In a steady-state oscillation, the attenuation coefficient measures the width of the resonance peak at $1/\sqrt{2}$ of the maximum amplitude, and Q measures its relative width: $\Delta f_{1/2} = \chi/\pi = f_0/Q$. Example with $Q = 10$ is shown.

Figure 3. Ray propagator in a layered medium (Equation 8). Geometrical spreading is related to the ratio of wavefront curvatures (gray dashed lines) at the receiver (R) and source (S).

Figure 4. One-dimensional plane-wave reflection-transmission problem. Solid lines are reflectors, dashed lines – incident-wave wavefronts at times t and $t + \delta t$, respectively. Multiple reflections are ignored.

Figure 5. Transmission responses of a simulated 100-boundary sequence [modified after Richards and Menke, 1983]: (a) transmitted record resulting from a single initial pulse; (b) power spectrum of its initial part (main pulse with early forward scattering, (c) spectrum of the later forward-scattered waves.

Figure 6. One-dimensional scattering problem: (a) on a single boundary, (b) on a random sequence of boundaries.

Figure 7. Random Gaussian distribution of impedance corresponding to mean velocity of 3.0 km/s and standard deviation of 0.25 km/s. The impedance is normalized to a mean value of $Z = 1.0$.

Figure 8. Wave attenuation in three statistical realizations of impedance time series (Figure 7) for frequency $f = 0.2 f_N$. Black and gray lines show the transmitted and reflected power, respectively.

Figure 9. Transmitted (black) and reflected (gray) power averaged over 100 statistical realizations as in Figure 8.

Figure 10. Frequency dependence of attenuation coefficient χ in 1-D propagation. Gray: propagation in a sequence of layers with equal travel times; black: propagation in layers with travel-times distributed according to a log-normal distribution. Dashed

line corresponds to the level of "scattering Q" equal 170.

Figure A1. Apparent attenuation for four spherically-symmetric global Rayleigh-wave models: a) in $Q(f)$ form, b) in $\chi(f)$ form. Model labels: DE [Dalton and Ekström, 2006], PREM [Dziewonski and Anderson, 1981], QL6 [Durek and Ekström, 1996], and QM1 [Widmer *et al*., 1991]. Note that $\chi(f)$ for PREM is near linear across the entire 50–250-s period band.

Figures

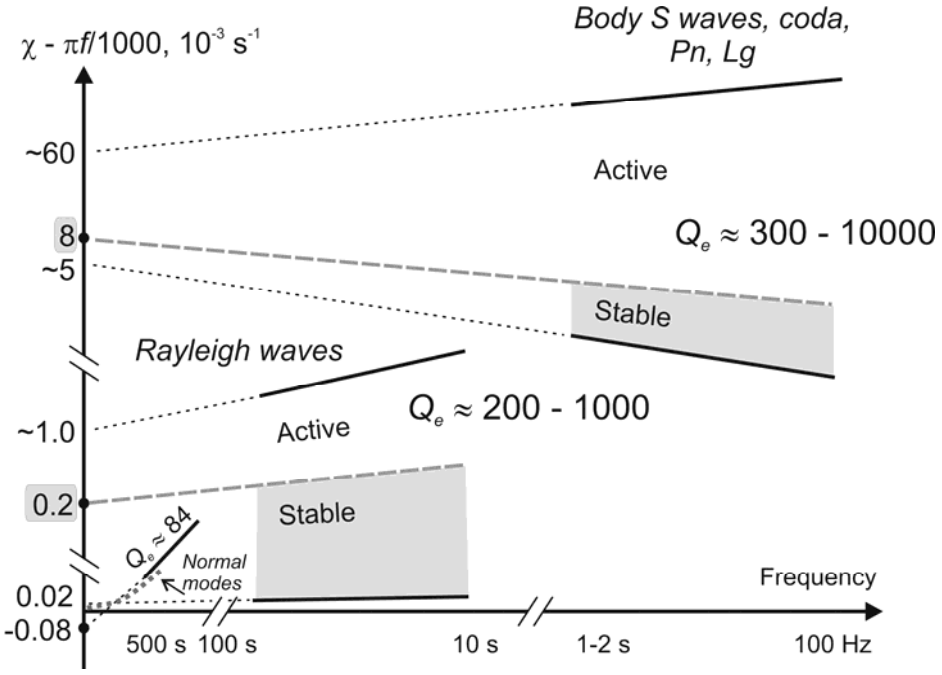

Figure 1. Summary of observed $\chi(f)$ dependences for Rayleigh waves and short-period body, *Lg*, *Pn*, and coda waves. "Reduced" values of (χ - πf/1000) are shown, so that the linear dependences corresponding to Q_e = 1000 appear horizontal. Typical ranges of Q_e, and γ levels discriminating between the stable and active tectonic regimes are indicated by lines and gray boxes, respectively. Modified from M10b, with permission from Springer.

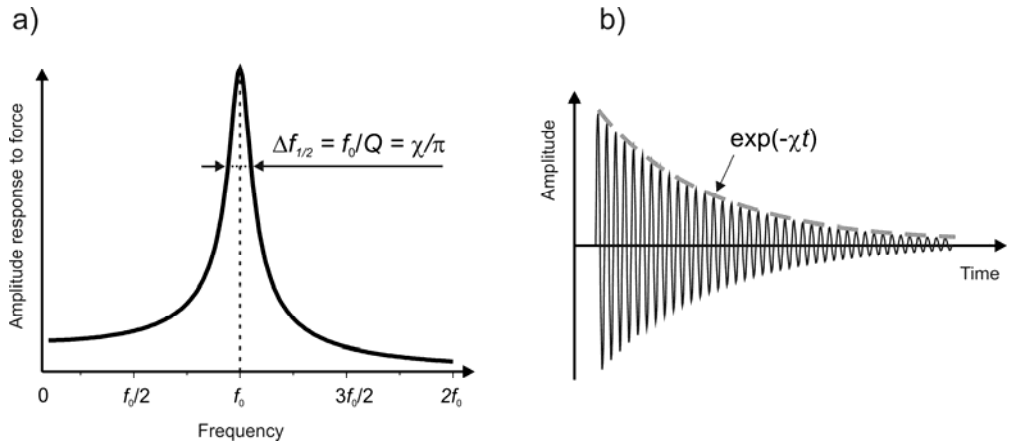

Figure 2. Definition of the attenuation coefficient, χ, and quality factor, Q, for an oscillatory process in: (a) frequency-domain, (b) time-domain. In a steady-state oscillation, the attenuation coefficient measures the width of the resonance peak at $1/\sqrt{2}$ of the maximum amplitude, and Q measures its relative width: $\Delta f_{1/2} = \chi/\pi = f_0/Q$. Example with $Q = 10$ is shown.

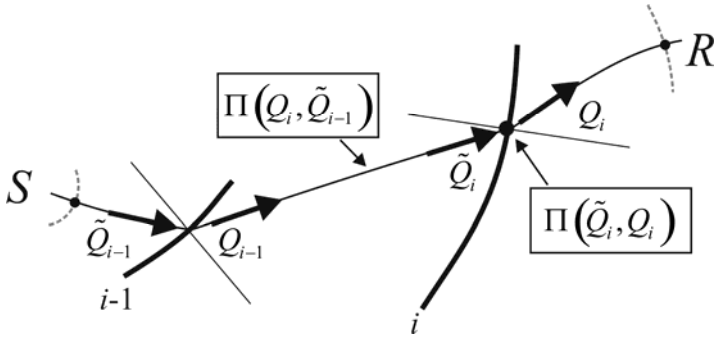

Figure 3. Ray propagator in a layered medium (Equation 8). Geometrical spreading is related to the ratio of wavefront curvatures (gray dashed lines) at the receiver (R) and source (S).

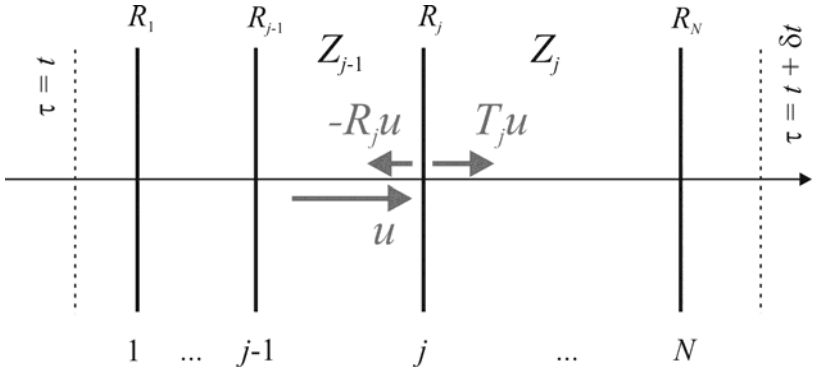

Figure 4. One-dimensional plane-wave reflection-transmission problem. Solid lines are reflectors, dashed lines – incident-wave wavefronts at times t and $t + \delta t$, respectively. Multiple reflections are ignored.

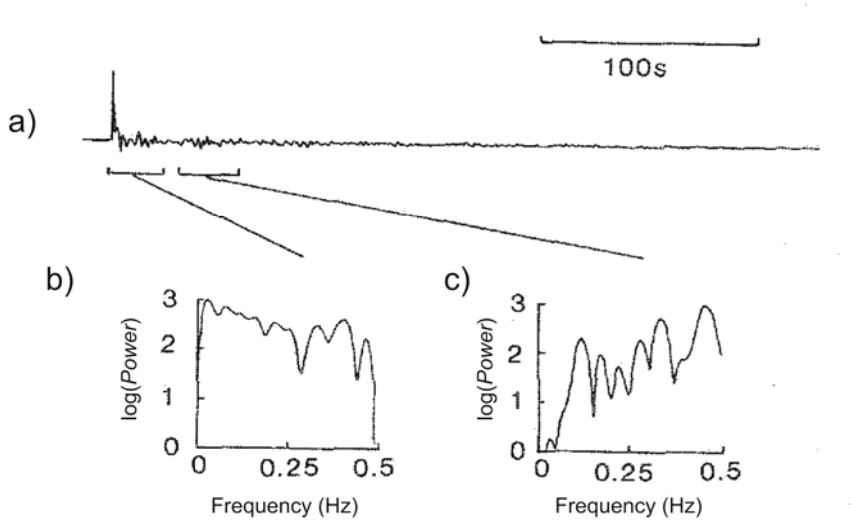

Figure 5. Transmission responses of a simulated 100-boundary sequence [modified after Richards and Menke, 1983]: (a) transmitted record resulting from a single initial pulse; (b) power spectrum of its initial part (main pulse with early forward scattering, (c) spectrum of the later forward-scattered waves.

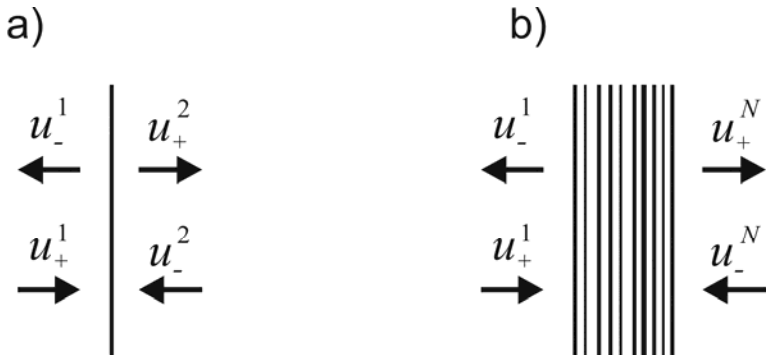

Figure 6. One-dimensional scattering problem: (a) on a single boundary, (b) on a random sequence of boundaries.

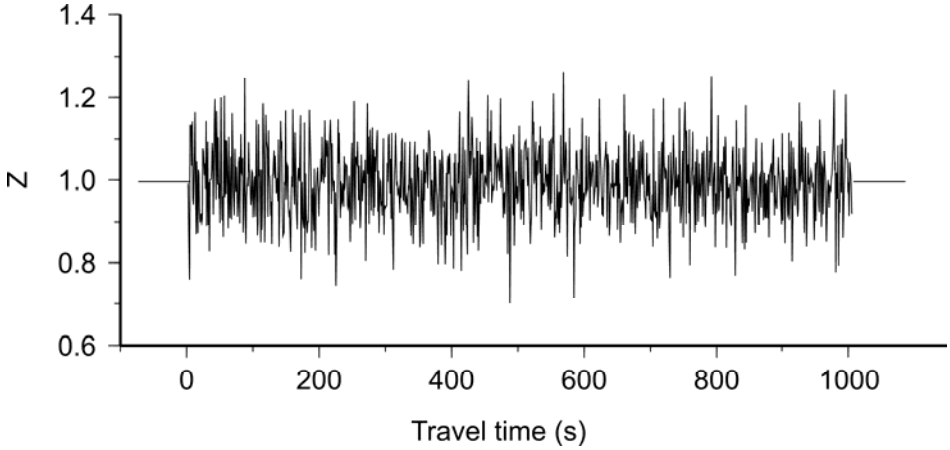

Figure 7. Random Gaussian distribution of impedance corresponding to mean velocity of 3.0 km/s and standard deviation of 0.25 km/s. The impedance is normalized to a mean value of $Z = 1.0$.

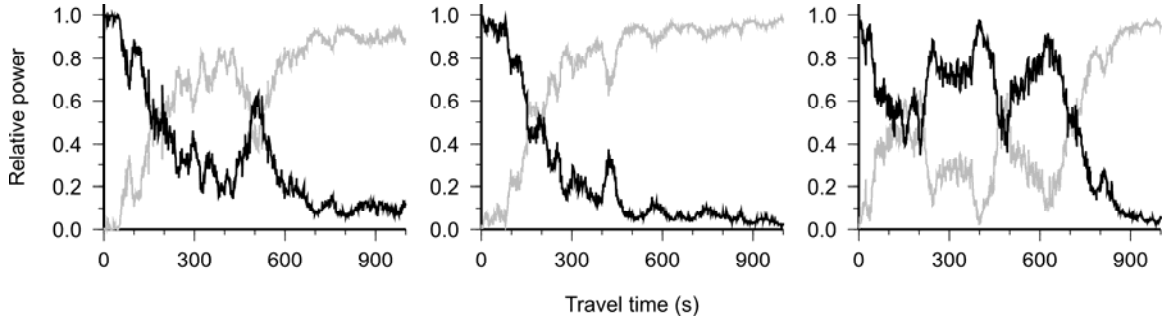

Figure 8. Wave attenuation in three statistical realizations of impedance time series (Figure 7) for frequency $f = 0.2f_N$. Black and gray lines show the transmitted and reflected power, respectively.

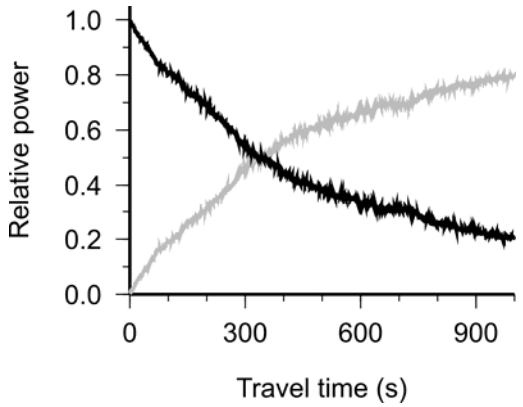

Figure 9. Transmitted (black) and reflected (gray) power averaged over 100 statistical realizations as in Figure 8.

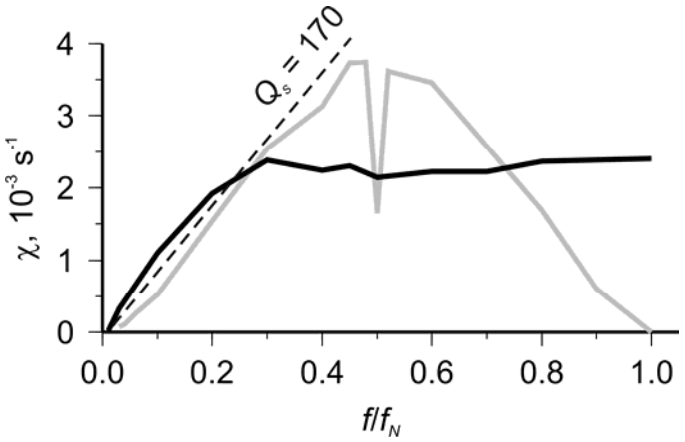

Figure 10. Frequency dependence of attenuation coefficient χ in 1-D propagation. Gray: propagation in a sequence of layers with equal travel times; black: propagation in layers with travel-times distributed according to a log-normal distribution. Dashed line corresponds to the level of "scattering *Q*" equal 170.

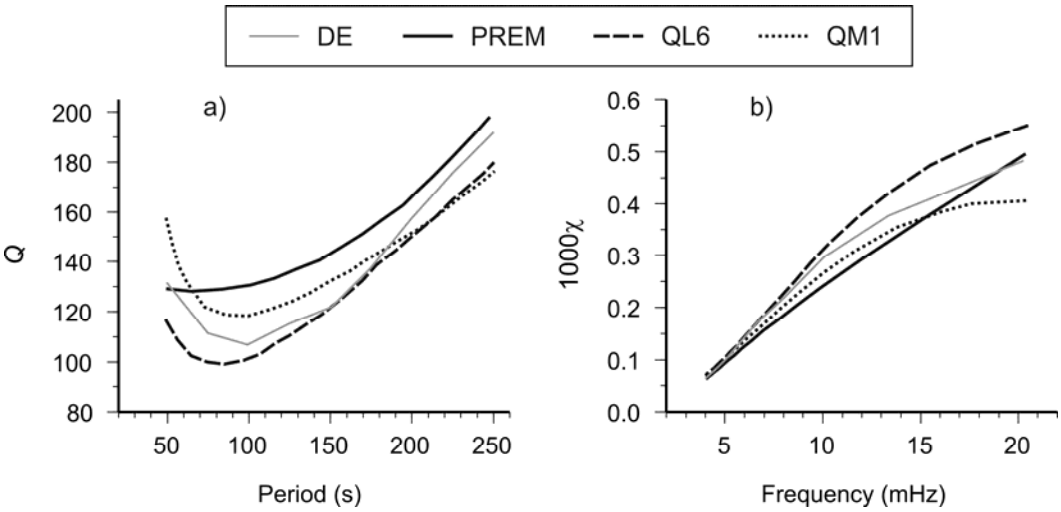

Figure A1. Apparent attenuation for four spherically-symmetric global Rayleigh-wave models: a) in $Q(f)$ form, b) in $\chi(f)$ form. Model labels: DE [Dalton and Ekström, 2006], PREM [Dziewonski and Anderson, 1981], QL6 [Durek and Ekström, 1996], and QM1 [Widmer *et al*., 1991]. Note that $\chi(f)$ for PREM is near linear across the entire 50–250-s period band.

Appendix A: Physical basis of the (γ, Q_e) model

Even if taken purely empirically, the (γ, Q_e) model (1) leads to two important general observations:

A) the geometrical spreading (GS) is typically not known accurately enough in order to measure the frequency dependence of Q;

B) GS variations can and should be estimated from the data, and it represents a most valuable attribute for interpretation.

These observations were illustrated on a number of datasets from ~500-s to ~100-Hz frequency bands and led to major reconsideration of several interpretations [M08, M09a, b, M10a–c]. Nevertheless, Xie and Fehler [2009] and Xie [2010, hereafter X10] argue that this literally cannot be done and present an extensive critique of this model. Their critique follows several lines, from the functional form of Equation (1) and data fitting to the physical meaning of geometrical attenuation and its relation to the viscoelastic theory and laboratory observations. At the same time, these authors do not address the key points A)–B) above and appear to misunderstand or misrepresent a number of other key points of the $\chi(f)$ approach. It is therefore important to compare the conventional and new model (1) in light of the argument by Xie and Fehler [2009] and X10.

A.1 Data fitting and criteria for model validity

It is known [*e.g.*, M08, M10a, X10] that seismic attenuation data can often be fit by using either the frequency-dependent $Q(f) = Q_0 f^{\eta}$ (*i.e.*, $\chi(f) = \pi f^{1-\eta}/Q_0$) or linear $\chi(f)$ dependences of the type (1). In M08, a mapping between parameters (γ, Q_e) and (Q_0, η) was derived, which was also sensitive to the observation frequency band.

With the existing datasets, two-parameter frequency dependencies are likely all that can be reliably constrained, and model (1) can be viewed as exploiting this fact by using a Maclaurin series in f [M08]. The traditional power-law $\chi(f) = \pi f^{1-\eta}/Q_0$ is another way to fit the $\chi(f)$ data with two parameters, although in a far less intuitive fashion. From the equivalence of these forms in data fitting, X10 argues that the observations of linear $\chi(f)$ dependencies "do not invalidate" the power-law $Q(f)$. Indeed, Equation (1) cannot invalidate the power-law or any other form of $Q(f)$; nevertheless, in view of its fitting the data well (in fact, often within broader frequency ranges than the power law [M08, M10a]), we can ask why a $Q(f)$ would really be required. This remains the key question, because it appears that the frequency-dependent Q is only motivated by the viscoelastic theory.

The true reasons for using one or another attenuation model are not in the data fit but in their correspondence to the physics of wave propagation [M10a]. As noted below, for viscoelasticity and Q, such correspondence can be seriously questioned. On the other hand, rigorous physical theories of waves in heterogeneous and attenuative media exist and do not require the use of an *in situ Q* [Biot, 1962].

A.2 Measured versus assumed geometrical spreading

The conventional practice of attenuation measurements defended by Xie and Fehler [2009] and X10 is based on the presumption that the GS can be established by mathematical modeling and *does not need to be measured*. In the notation of this paper, this means that γ in Equations (2) and (4) can always be taken equal zero. However, a realistic GS is practically impossible to define mathematically. Any controlled-source data section shows that "multi-pathing" (*i.e.*, reflections, refractions, and mode conversions) is so pervasive that the wavefronts that could be followed for GS prediction are completely absent. At the same time, despite the lack of tractable mathematical formulations, the GS certainly exists as a physical process, and its parameters can be measured as described in M08, M10a, and M10b. In practical observations, we only have the frequency-dependent attenuation coefficient to go by, and therefore we can only approximate the residual GS as a frequency-independent part of the attenuation coefficient, which is given by parameter γ. For the same reason, the effects of small-scale scattering cannot be unambiguously separated from this residual GS [M08, M10a].

A.3 Physical basis of γ

While criticizing the general idea of variable and measured GS, X10 focuses on the exponential form of the correction to G_0:

$$G = G_0 \delta G \equiv G_0 e^{-\gamma t}, \tag{A1}$$

which arises from Equation (2) with $f = 0$. Here, G is the true GS within the structure, G_0 is the assumed reference GS, and we call δG the "residual GS" [M08, M10a]. According to X10, this functional form for G has "no physical basis," principally because of its decaying too quickly at large times. However, as explained in M10a, Equation (2) represents a common perturbation- (or scattering-) theory approximation, which only means that the rate of GS variation, $\delta G/\delta t$, is small and proportional to G. Similarly to all perturbation models, this approximation *should not* be used at the limit of $t \to \infty$, in which a diffusive (also called multiple-scattering) regime establishes. Maybe not appreciating this point, X10 applies the $\delta G = e^{-\gamma t}$ correction to ~300-km distances (Appendices 1 and 2 in that paper), whereas it was only proposed for up to 50–70 km, and also uses exaggerated values of γ. If the limit $t \to \infty$ is not considered, then both functional forms G_0 and $G_0 e^{-\gamma t}$ in Equation (A1) are equally acceptable, because G_0 itself is also only some *ad hoc*, or reference approximation for the GS. Other forms of GS corrections were also proposed in M10a, with the exponential model (A1) preferred because of its useful roots in the scattering approximation.

It is clearly impossible to disprove the validity of approximation (A1), because the realistic baseline G_0 has neither unique functional form nor definite physical meaning. In his Appendix 2, X10 offers an example of a "physically meaningful" GS of a wavefront spreading in a 2-D structure with a linear velocity gradient. However, this derivation is incorrect, because it assumes that the wavefront remains cylindrical in shape while propagating at different speeds in different directions. This once again illustrates the fundamental difficulty of purely mathematical approaches to GS.

A.4 Accuracy of perturbation-theory approximation

Many studies show that the theoretical, GS approximation G_0 is often inaccurate and affects the attenuation measurements, which is known as the "trade-off" of Q with the assumed model GS [*e.g.*, Kinoshita, 1994]. In M08 and related papers, this notion of a model trade-off was viewed as unacceptable and the accuracy of G_0 was tested quantitatively by using ansatz (1) as a single-parameter generalization of the conventional G_0. The data showed that γ were non-zero in most cases, and also that the entire frequency-dependent part of Q can be absorbed by a correction in γ. This correction also increases the values of Q (from Q_0 to Q_e) by as much as ~20–30 times [M08, M10a]. Thus, the zero-order approximation G_0 is clearly insufficiently accurate for measuring the *in situ* Q.

The next important question is whether the first-order correction (1) to G_0 is accurate enough. X10 correctly notes that from some datasets, $|\gamma|$ values turn out to be too large and violate the perturbation-theory criterion $t|\gamma| << 1$, where t is the characteristic observation time [M10a]. However, from such large γ values, X10 makes a paradoxical conclusions that one should therefore use G_0 (*i.e.*, set $\gamma = 0$) and that the attenuation measurements "cannot be improved" by a better GS model. On the contrary, large $|\gamma|$ only means that G_0 is too inaccurate, and a correction *is* required. With the use of a more accurate G_0, such as the numeric models of M10a, the values of γ would reduce, and approximation (1) would enter the range of its formal validity.

Finally, Q represents only a second-order effect which can only be constrained when both G_0 and the residual GS (γ) are accounted for. It appears that realistically, this can only be done based on the frequency dependence of χ, *i.e.*, by measuring Q_e from the spectral slopes of seismic amplitudes. This can only be done by assuming that the residual GS is frequency independent [M10a].

A.5 Monotony of apparent $Q(f)$ dependencies

In a peculiar but instructive argument that deserves some discussion, X10 finds a "fundamental contradiction" of the $\chi(f)$ model (1) in the fact that it only predicts apparent $Q = \pi f/\chi$ values monotonously varying with frequency. X10 points out that among the four major long-period Rayleigh-wave models, only PREM [Dziewonski and Anderson, 1981] shows a monotonous increase of the apparent Q with f (Figure A1a). However, all four models cannot be correct simultaneously, and they differ among themselves to about the same extent as from PREM. Therefore, all of these models do not have to comply with model (1). At the same time, note that PREM shows an almost perfectly linear $\chi(f)$ dependence within the entire frequency band (Figure A1b).

As Figure 10 shows, χ and even more so Q are not required to vary monotonously with frequency in model (1). Values γ and Q_e in Equations (1) and (4) are apparent quantities, and their constancy is just an empirical observation for certain wave types and frequency bands [M08]. At the same time, it is certainly remarkable that these quantities stay nearly constant within the same wave types [M10b and Section 3 here].

A.6 Lab observations of frequency-dependent *Q*

An important argument in favor of a frequency-dependent *Q* and implicitly against the attenuation-coefficient model (1) comes from lab measurements using rock samples [X10]. Indeed, many lab observations at seismological frequencies, such as by Faul *et al*. [2004], yield values of *Q* increasing with frequencies. Nevertheless, one should not think that the GS does not exist in lab experiments, or that such measurements are unaffected by elastic structural effects. Quite oppositely, the transformation of the measured quantities, which are the resonance-peak widths or strain-stress phase delays, into the inferred "material *Q*" is most complex for lab data and relies on the most intricate models and numerous corrections [Bourbié *et al*., 1987]. These models cause pronounced effects in the elastic limit (see Section 3) and play the role of the GS. The examples in Section 3 of this paper illustrate three types of such effects quantitatively.

A.7 Physical basis of conventional attenuation models

Ironically, the physical basis of the conventional GS and *Q* models (such as $G_0 \propto t^{-\nu}$ and $Q = Q_0 f^{\eta}$, respectively) is much more difficult to establish than that of the perturbation-theory formulas (1) and (4). Both of these models only arise in overly simplified theories, such as the approximations of the Earth's lithosphere as a uniform and isotropic half-space with a flat boundary commonly used in local-coda studies [*e.g*., Aki, 1980]. The $Q_0 f^{\eta}$ power law appears to be suggested by the elementary "equivalent linear solid" models [*e.g*., Carcione, 2007], but at the same time, multiple solids are usually superimposed to allow *almost arbitrary* frequency dependencies of *Q* [Liu *et al*., 1976]. The only definite constraint on possible $\chi(f) = \pi f/Q$ dependencies from the power-law *Q* model consists in $\chi|_{f\to 0} = 0$. However, such a constraint is not physically justified and is commonly violated in observations [M08, M09a, M10].

It appears that the reason for the popularity of *Q* in attenuation models is not in its physical validity but in simplicity, flexibility, and practical convenience. Once we postulate that virtually the same quantity, namely Q^{-1}, exists as both the material and observed (apparent) property, the theory becomes greatly simplified. The correspondence principle [Aki and Richards, 2002] allows treating the *in situ* $Q^{-1}/2$ as a complex argument of the velocity, which dramatically simplifies modeling and inversion. The frequency dependence of the *in situ Q* provides a very flexible parameterization which allows fitting and modeling the data across broad frequency bands. However, all this is achieved by departing from the mechanical description of the medium, which means that such a *Q* may be no more than a heuristic mathematical model.

A.8 In situ *Q* and viscoelasticity

The viscoelastic theory is often used for an implicit conceptual support for a frequency-dependent *in situ Q* of the propagating medium [X10]. This is a very extensive subject that cannot be fully addressed here; however, two observations regarding this support were made in M09b. First, note that the quality factor was introduced in seismology from an intuitive analogy with acoustic or mechanical resonators [Knopoff, 1964] but it is still not the type of quantity that can be easily associated with a point within the medium. The difficulty of defining a "material *Q*" can be seen from the

fact that there exist many factors responsible for elastic-energy dissipation, such as the rock-matrix properties, grain shapes, pore volumes, shapes and connectivity, fractures, fluids, and various dielectric and piezoelectric properties. Most of these factors are unrelated to the elastic moduli and cannot be lumped into the only two values of Q_K and Q_μ used in the traditional seismic viscoelasticity. Thus, the viscoelastic model is far *too simple* to describe the real Earth materials.

Second, the viscoelastic model is also *too general* and permissive. It only reproduces the formal convolutional relationships between the strain and stress within a wave but does not constrain the mechanism of energy dissipation. However, nearly any linear process can be presented as "viscoelastic" in this sense. For example, the ordinary Newtonian mechanics can be described by convolutional integrals relating the particle position, $x(t)$, to the force-rate history, $\dot{f}(t)$:

$$x(t) = \int_{-\infty}^{t} J(t-\tau)\, \dot{f}(\tau)\, d\tau , \tag{A2}$$

where $J(t)$ can be called the "retarded compliance function:"

$$J(t) = \frac{\theta(t)}{2m} t^2 , \tag{A3}$$

m is the mass, and $\theta(t)$ is the Heavyside step function. However, such a picture does not replace the second Newton's law, $\ddot{x}(t) = f(t)/m$, and should not be interpreted literally, as some "memory" inherent in particle motion. Note the similarity of Equation (A2) to the viscoelastic relation of the strain, ε, to stress-rate history, $\dot{\sigma}$ [Dahlen and Tromp, 1998]:

$$\varepsilon(t) = \int_{-\infty}^{t} J(t-\tau)\, \dot{\sigma}(\tau)\, d\tau . \tag{A4}$$

Another fundamental problem in applying the viscoelasticity to seismology is the absence of a unique definition for the elastic energy [*e.g.*, Carcione, 2007]. This leads to the absence of the traditional Hamiltonian dynamic principle, which is standard in mechanics. Among its practical manifestations, this problem leads, for example, to an incorrect complex argument of the acoustic impedance in the presence of attenuation [M10c].